RESEARCH ARTICLE SUMMARY

NEUROEVOLUTION

Single-cell Stereo-seq reveals induced progenitor cells involved in axolotl brain regeneration

Xiaoyu Wei†, Sulei Fu†, Hanbo Li*†, Yang Liu†, Shuai Wang†, Weimin Feng†, Yunzhi Yang†, Xiawei Liu, Yan-Yun Zeng, Mengnan Cheng, Yiwei Lai, Xiaojie Qiu, Liang Wu, Nannan Zhang, Yujia Jiang, Jiangshan Xu, Xiaoshan Su, Cheng Peng, Lei Han, Wilson Pak-Kin Lou, Chuanyu Liu, Yue Yuan, Kailong Ma, Tao Yang, Xiangyu Pan, Shang Gao, Ao Chen, Miguel A. Esteban, Huanming Yang, Jian Wang, Guangyi Fan, Longqi Liu, Liang Chen*, Xun Xu*, Ji-Feng Fei*, Ying Gu*

INTRODUCTION: Brain regeneration requires the coordination of complex responses in a time- and region-specific manner. Identifying the cell types and molecules involved in this process would advance our understanding of brain regeneration and provide potential targets for regenerative medicine research. However, progress in this field has been hampered by the limited regeneration capacity of the mammalian brain and an incomplete mechanistic understanding of the regeneration process at both the cellular and molecular levels. Axolotls (*Ambystoma mexicanum*) can regenerate damaged appendages and multiple internal organs, including the brain. Therefore, axolotls may serve as a model for studying brain regeneration.

RATIONALE: If we are to understand the mechanism of brain regeneration, we need research tools that can achieve large-scale data acquisition and analyses to simultaneously decode complex cellular and molecular responses. It also seemed to us that a comparison between brain regeneration and developmental processes would help to provide new insights into the nature of brain regeneration. Accordingly, we removed a small portion of the lateral pallium region of the axolotl left telencephalon and collected tissue samples at multiple stages during regeneration. In parallel, we collected tissue samples of the axolotl telencephalon at multiple developmental stages. We then used high-definition and large-field Stereo-seq (spatial enhanced resolution omics sequencing) technology to generate spatial transcriptomic data from sections that covered both hemispheres of the axolotl telencephalon at single-cell resolution. Analyses of cell type annotation, cell spatial organization, gene activity dynamics, and cell state transition were performed for a mechanistic investigation of injury-induced regeneration compared to these cell attributes during development.

RESULTS: With the use of Stereo-seq, we generated a group of spatial transcriptomic data of telencephalon sections that covered six developmental and seven injury-induced regenerative stages. The data at single-cell resolution enabled us to identify 33 cell types present during development and 28 cell types involved in regeneration, including different types of excitatory and inhibitory neurons, and several ependymoglial cell subtypes. For development, our data revealed a primitive type of ependymoglial cells that may give rise to three subgroups of adult ependymoglial cells localized in separate areas of the ventricular zone, with different molecular features and potentially different functions. For regeneration, we discovered a subpopulation of ependymoglial cells that may originate from local resident ependymoglial cells activated by injury. This population of progenitor cells may then proliferate to cover the wound area and subsequently replenish lost neurons through a state transition to intermediate progenitors, immature neurons, and eventually mature neurons. When comparing cellular and molecular dynamics of the axolotl telencephalon between development and regeneration, we found that injury-induced ependymoglial cells were similar to developmental-specific ependymoglial cells in terms of their transcriptome state. We also observed that regeneration of the axolotl telencephalon exhibited neurogenesis patterns similar to those seen in development in molecular cascades and the potential cell lineage transition, which suggests that brain regeneration partially recapitulates the development process.

CONCLUSION: Our spatial transcriptomic data highlight the cellular and molecular features of the axolotl telencephalon during development and injury-induced regeneration. Further characterization of the activation and functional regulation of ependymoglial cells may yield insights for improving the regenerative capability of mammalian brains. Our single-cell spatial transcriptome of the axolotl telencephalon, a tetrapod vertebrate, also provides data useful for further research in developmental, regenerative, and evolutionary brain biology. All data are accessible in an interactive database (https://db.cngb.org/stomics/artista). ■

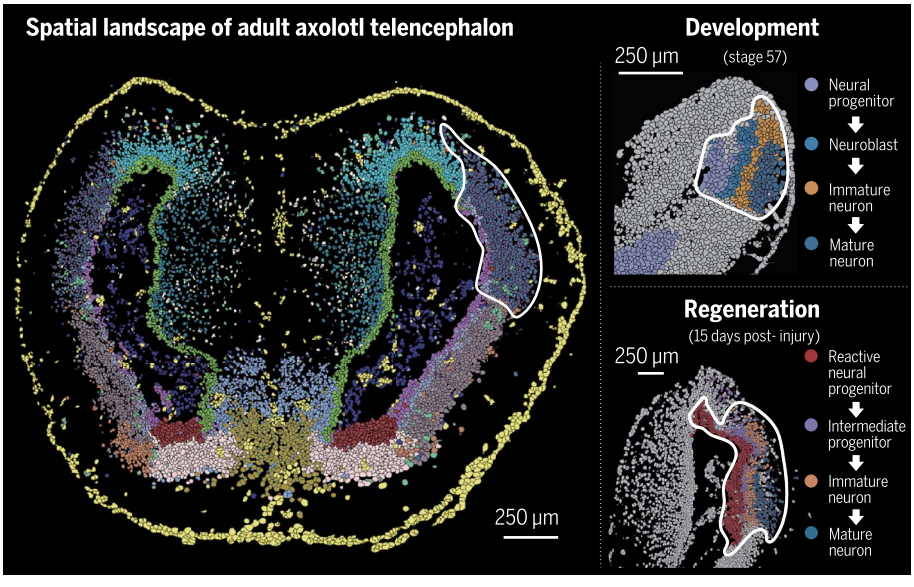

Development and regeneration of axolotl telencephalon. The spatially resolved single-cell transcriptome of the adult axolotl telencephalon as determined by Stereo-seq analyses (left). Upon brain injury in the highlighted lateral pallium region of the left hemisphere, a neural progenitor subpopulation at the wound site was rapidly induced and subsequently replenished lost neurons (bottom right) through a process that partially resembles neurogenesis during development (top right).

The list of author affiliations is available in the full article online.
*Corresponding author. Email: guying@genomics.cn (Y.G.); jifengfei@gdph.org.cn (J.-F.F.); xuxun@genomics.cn (X.X.); liang_chen@whu.edu.cn (L.C.); lihanbo@genomics.cn (H.L.)
†These authors contributed equally to this work.
Cite this article as X. Wei *et al.*, *Science* **377**, eabp9444 (2022). DOI: 10.1126/science.abp9444

READ THE FULL ARTICLE AT
https://doi.org/10.1126/science.abp9444

RESEARCH ARTICLE

NEUROEVOLUTION

Single-cell Stereo-seq reveals induced progenitor cells involved in axolotl brain regeneration

Xiaoyu Wei[1,2]†, Sulei Fu[3,4]†, Hanbo Li[2,5,6]*†, Yang Liu[2]†, Shuai Wang[2,7]†, Weimin Feng[2,7]†, Yunzhi Yang[8]†, Xiawei Liu[5], Yan-Yun Zeng[3,4], Mengnan Cheng[2,7], Yiwei Lai[9], Xiaojie Qiu[10,11], Liang Wu[2,7], Nannan Zhang[5], Yujia Jiang[2,8], Jiangshan Xu[2,7], Xiaoshan Su[5], Cheng Peng[3,4], Lei Han[2,12,13], Wilson Pak-Kin Lou[3,4], Chuanyu Liu[2,13], Yue Yuan[2,7], Kailong Ma[2], Tao Yang[2], Xiangyu Pan[3], Shang Gao[5], Ao Chen[2,14], Miguel A. Esteban[9,15], Huanming Yang[2,16], Jian Wang[2,16], Guangyi Fan[2], Longqi Liu[1,2,7,13], Liang Chen[17]*, Xun Xu[2,18]*, Ji-Feng Fei[3]*, Ying Gu[1,2,7,18]*

The molecular mechanism underlying brain regeneration in vertebrates remains elusive. We performed spatial enhanced resolution omics sequencing (Stereo-seq) to capture spatially resolved single-cell transcriptomes of axolotl telencephalon sections during development and regeneration. Annotated cell types exhibited distinct spatial distribution, molecular features, and functions. We identified an injury-induced ependymoglial cell cluster at the wound site as a progenitor cell population for the potential replenishment of lost neurons, through a cell state transition process resembling neurogenesis during development. Transcriptome comparisons indicated that these induced cells may originate from local resident ependymoglial cells. We further uncovered spatially defined neurons at the lesion site that may regress to an immature neuron–like state. Our work establishes spatial transcriptome profiles of an anamniote tetrapod brain and decodes potential neurogenesis from ependymoglial cells for development and regeneration, thus providing mechanistic insights into vertebrate brain regeneration.

Mammals face challenges in recovering from brain injury because of their limited regeneration capability (*1*). In contrast, lower vertebrates, such as teleost fish and salamanders, exhibit regenerative power (*2*–*7*). Forebrain regeneration in axolotls was first observed in larvae (*8*) and later in adults (*4*, *9*). Lost cortical cell types in the axolotl telencephalon could apparently be restored upon injury (*9*). Therefore, axolotls may serve as a model for studying brain regeneration, possibly leading to discoveries that could be valuable for understanding the inherent limitations of brain regeneration in mammals and, ultimately, developing regenerative medicine for the central nervous system.

Previous studies in various regenerative species have shown that ependymoglial cells (EGCs), equivalent to neural stem cells in mammals, contribute to neurogenesis during brain regeneration (*3*, *10*, *11*). Salamander EGCs may give rise to nearly all cell types in the brain during development (*12*). Unlike mammals, in which neural stem cells are almost consumed once brain development is complete, except those in the subventricular zone and hippocampal dentate gyrus, the adult salamander contains dividing EGCs in the brain (*1*, *13*). EGCs are distributed in the entire ventricular zone (VZ) of adult axolotl brains, as well as in a few confined regions of the VZ in red spotted newts (*10*). It has been reported that red spotted newts harbor two groups of EGCs: slow-dividing and transient amplifying EGCs (*10*). The first group is stem cell–like, expressing glial fibrillary acidic protein (GFAP) and glutamine synthetase (*3*, *14*) and showing the stem cell property of long-term 5-bromo-2′-deoxyuridine (BrdU) retention. The second group is located within the proliferative hot spots of the VZ and frequently divides (*10*). Both EGC groups can react to injury and can expand to larger areas in the pallium (*4*, *10*).

So far, the role and regulation of EGCs in regeneration have only been partially characterized. A few signaling pathways in EGC activation and brain regeneration have been documented in salamanders and fish, such as Notch, FGF, and Gata3 (*10*, *15*, *16*); these are also involved in brain development, indicating that brain regeneration and development may possess similar molecular regulations. However, it remains unknown whether and to what extent brain regeneration recapitulates embryonic development. Therefore, a more systematic characterization of cellular and molecular functions is needed that substantiates the mechanistic understanding of brain regeneration.

Several spatial transcriptomic technologies suitable for dissecting the development and tissue regeneration processes have been developed to resolve gene expression profiles of cells in situ (*17*). By these approaches, the in situ transcriptome profiles of mouse brain or human cortex have been resolved at resolutions of 100 and 55 μm, respectively, which reflect the average expression profiles of a group of neighboring cells (*18*, *19*). Considering the complexity of brain structures and cell types, improved resolution of transcript capturing is needed to enhance the accuracy of data interpretation. Sequential fluorescence in situ hybridization (FISH) and multiplexed error-robust FISH were developed to profile gene expression in single cells, but their application is limited by low throughput and the requirement for special equipment (*20*, *21*).

Using spatial enhanced resolution omics sequencing (Stereo-seq) (*22*), we determined spatially resolved single-cell transcriptomes of axolotl telencephalon sections at a series of developmental and regeneration stages. These data enabled us to identify cell types, including EGC subtypes involved in development and regeneration. Further analyses showed that developmental and regenerative neurogenesis shared similarities in cell lineage dynamics from EGCs to mature neurons and related molecular signatures. We also observed a wound-stimulated cell cluster adjacent to EGCs with neuronal regression features. Taken together, our work provides an overview of the cellular dynamics during axolotl brain development and regeneration, the datasets from which may yield insights into the molecular regulation of brain regeneration.

Stereo-seq profiles spatial transcriptomes of axolotl telencephalons

Considering the average size of axolotl cells, we prepared cryosections of the adult axolotl telencephalon at 20-μm thickness to capture roughly a single-cell layer of tissue for Stereo-seq analysis on the entire section (Fig. 1A)

[1]BGI-Hangzhou, Hangzhou 310012, China. [2]BGI-Shenzhen, Shenzhen 518103, China. [3]Department of Pathology, Guangdong Provincial People's Hospital, Guangdong Academy of Medical Sciences, Guangzhou 510080, China. [4]Key Laboratory of Brain, Cognition and Education Sciences, Ministry of Education, Institute for Brain Research and Rehabilitation, South China Normal University, Guangzhou 510631, China. [5]BGI-Qingdao, Qingdao 266555, China. [6]Lars Bolund Institute of Regenerative Medicine, Qingdao-Europe Advanced Institute for Life Sciences, BGI-Qingdao, Qingdao 266555, China. [7]College of Life Sciences, University of Chinese Academy of Sciences, Beijing 100049, China. [8]BGI College & Henan Institute of Medical and Pharmaceutical Sciences, Zhengzhou University, Zhengzhou 450000, China. [9]Laboratory of Integrative Biology, Guangzhou Institutes of Biomedicine and Health, Chinese Academy of Sciences, Guangzhou 510530, China. [10]Whitehead Institute for Biomedical Research, Cambridge, MA 02142, USA. [11]Howard Hughes Medical Institute, Massachusetts Institute of Technology, Cambridge, MA 02139, USA. [12]Shenzhen Key Laboratory of Single-Cell Omics, BGI-Shenzhen, Shenzhen 518120, China. [13]Shenzhen Bay Laboratory, Shenzhen 518000, China. [14]Department of Biology, University of Copenhagen, Copenhagen DK-2200, Denmark. [15]Institute of Stem Cells and Regeneration, Chinese Academy of Sciences, Beijing 100101, China. [16]James D. Watson Institute of Genome Sciences, Hangzhou 310058, China. [17]Hubei Key Laboratory of Cell Homeostasis, RNA Institute, College of Life Sciences, Wuhan University, Wuhan 430072, China. [18]Guangdong Provincial Key Laboratory of Genome Read and Write, BGI-Shenzhen, Shenzhen 518120, China.
***Corresponding author. Email: guying@genomics.cn (Y.G.); jifengfei@gdph.org.cn (J.-F.F.); xuxun@genomics.cn (X.X.); liang_chen@whu.edu.cn (L.C.); lihanbo@genomics.cn (H.L.)**
†These authors contributed equally to this work.

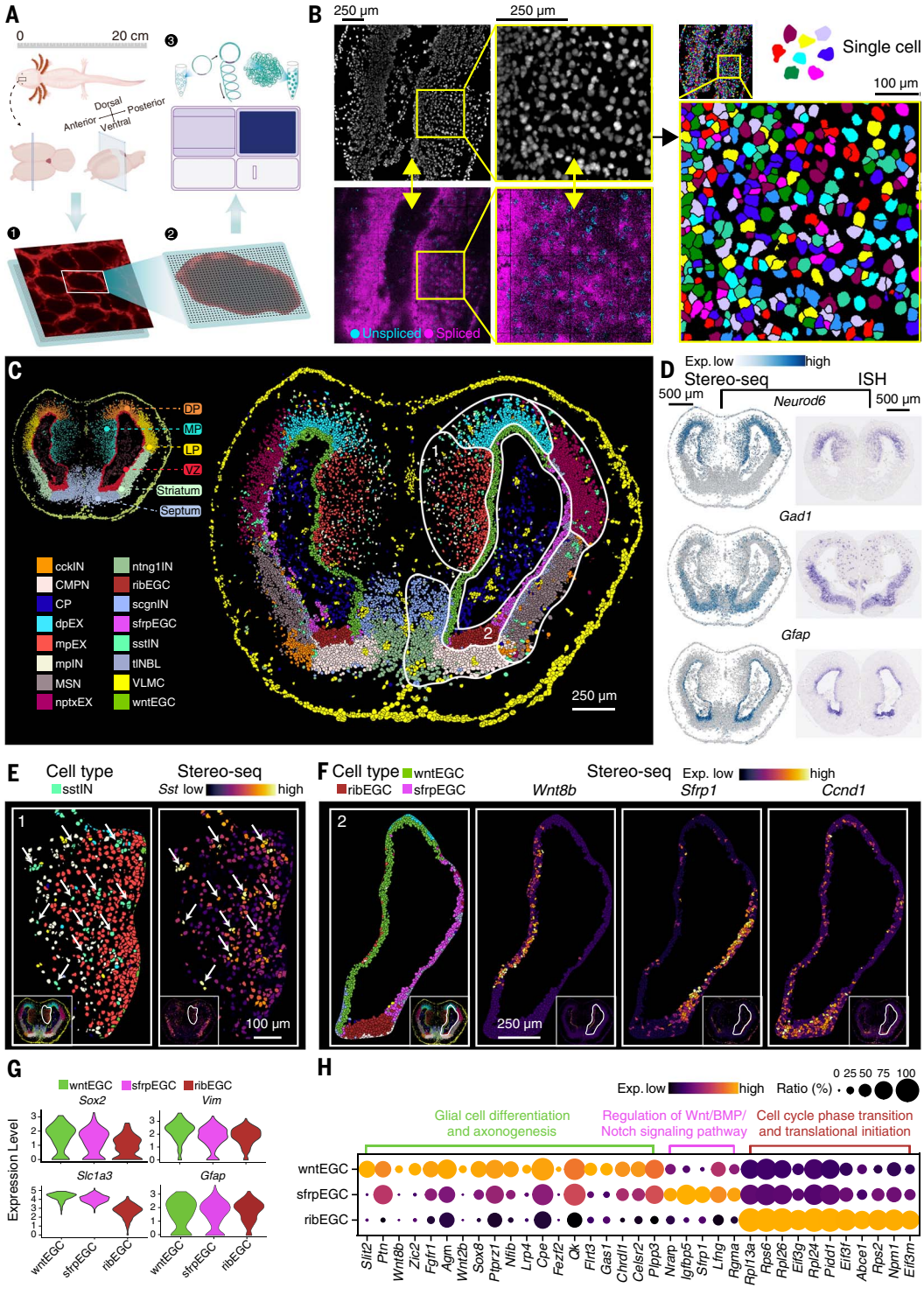

Fig. 1. Spatial transcriptome of axolotl telencephalon by Stereo-seq. (**A**) Schematic diagram of Stereo-seq for the axolotl telencephalon. Step 1: sample collection and frozen section preparation of the adult axolotl telencephalon. Step 2: in situ RNA capture of tissue loaded onto the Stereo-seq chip. Step 3: cDNA amplification, library construction, and sequencing. (**B**) Spatially assigned spliced (purple) and unspliced transcripts (blue) (bottom left) and corresponding nucleus areas represented by single-stranded DNA staining (gray) (top left). Single-cell segmentations were performed by watershed algorithm (right). (**C**) Stereo-seq identified anatomical regions (top left) and cell types (right) of axolotl telencephalon. DP, dorsal pallium; MP, medial pallium; LP, lateral pallium; VZ, ventricular zone; cckIN, *Cck*$^{+}$ inhibitory neuron; CMPN, cholinergic, monoaminergic, and peptidergic neuron; CP, choroid plexus; dpEX, dorsal palliumexcitatory neuron; mpEX, medial pallium excitatory neuron; mpIN, medial pallium inhibitory neuron; MSN, medium spiny neuron; nptxEX, *Nptx*$^{+}$ lateral pallium excitatory neuron; ntng1IN, *Ntng1*$^{+}$ inhibitory neuron; ribEGC, ribosomal EGC; scgnIN, *Scgn*$^{+}$ inhibitory neuron; sfrpEGC, *Sfrp*$^{+}$ EGC; sstIN, *Sst*$^{+}$ inhibitory neuron; tlNBL, telencephalon neuroblast; VLMC, vascular leptomeningeal cell; wntEGC, *Wnt*$^{+}$ EGC. (**D**) Spatial visualization of the expression of selected genes on Stereo-seq maps (left) and corresponding RNA ISH images (right). (**E**) Distribution of the sstIN in the medial pallium region of the adult axolotl telencephalon. Annotated sstIN in green (left) and cells expressing high levels of the *Sst* gene (right) are indicated by white arrows. (**F**) The distribution of three subtypes of EGCs (left). The expression of marker genes for the selected EGC subtype is shown (right). (**G**) Violin plot showing the expression level of neural stem cell markers (*Sox2*, *Vim*, *Slc1a3*, and *Gfap*) in three types of EGCs. (**H**) Bubble plot showing the expression level of specific markers of various biological functions in each EGC subtype.

(*22*–*24*). Because Stereo-seq is based on DNA nanoball (DNB) sequencing technology (*25*), for which each DNB spot on the chip is 220 nm in diameter and the center-to-center distance of two adjacent spots is 500 or 715 nm, we were able to capture transcripts at the subcellular level (Fig. 1A and fig. S1A).

To mark the position of individual cells on the section, we performed DNA staining to highlight the nucleus, where newly transcribed pre-mRNAs undergo splicing (Fig. 1B, left panels) (*26*). Indeed, intron-containing transcripts were observed in nuclear regions and were separated from spliced transcripts (Fig. 1B, left panels). We then used the watershed algorithm to extract transcripts in each nucleus and its surrounding region, in which both nuclear and cytoplasmic transcript-containing areas were included for cell boundary demarcation. In this way, we were able to assign transcripts to individually defined cell areas,

achieving single-cell resolution (Fig. 1B, right panels, and fig. S1, B and C). Each cell area contained ~850 DNB spots, in which an average of 6291 unique molecular identifiers (UMIs) and 1680 genes were detected (fig. S1, D and E, and table S1).

To acquire a global picture of cell clusters spatially assigned onto the section, we performed the spatially constrained clustering analysis (see Methods). In total, we obtained six clusters of cells separated into previously defined anatomical regions of the axolotl telencephalon, including the VZ, dorsal pallium, medial pallium, lateral pallium, striatum, and septum (Fig. 1C, top left) (*3*, *13*, *27*). To dissect cell type composition, we next conducted unsupervised clustering analysis by Seurat based solely on gene expression (*28*). This analysis identified 16 cell clusters, which were further mapped to the section according to their spatial information (Fig. 1C, right). Referring to established cell marker genes, such as excitatory neuron marker *Neurod6*, inhibitory neuron marker *Gad1*, and EGC marker *Gfap* (Fig. 1D), we determined the identity of each cell cluster (fig. S2A and table S2). We further validated the spatial distribution of Stereo-seq signals for selected marker genes by RNA in situ hybridization (RNA ISH) (figs. S2B and S3).

Different cell types were distributed at distinct locations (Fig. 1C and fig. S4). Excitatory neurons, including dorsal pallium excitatory neurons, medial pallium excitatory neurons, and *Nptx*$^+$ lateral pallium excitatory neurons (nptxEXs), were enriched in the pallium. In contrast, inhibitory neurons, such as *Cck*$^+$ inhibitory neurons, medial pallium inhibitory neurons, medium spiny neurons, *Ntng1*$^+$ inhibitory neurons, *Scgn*$^+$ inhibitory neurons, and *Sst*$^+$ inhibitory neurons, were more abundant in the striatum, medial pallium, and septum regions and were physically separated from excitatory neurons (Fig. 1C and fig. S4).

Similar to other spatial transcriptomic techniques, sample processing for Stereo-seq may cause RNA transcripts to diffuse laterally to neighboring areas (*22*). We next examined whether this effect would interfere with cell type annotation. We chose *Sst*$^+$ inhibitory neurons for demonstration because they are sparsely distributed in the pallium (Fig. 1E and fig. S5A) (*9*). Although the *Sst* transcript indeed diffused in Stereo-seq data (Fig. 1E, right), its level dropped rapidly beyond cell boundaries (fig. S5B). Statistically, the average transcript levels of *Sst* and *Gad2* (another gene expressed in *Sst*$^+$ inhibitory neurons) were significantly lower in neighboring cells than in *Sst*$^+$ inhibitory neurons (fig. S5C). Therefore, we were able to achieve identification of *Sst*$^+$ inhibitory neurons (fig. S5D). We further evaluated RNA diffusion and cell type identification of Stereo-seq by comparison with RNA ISH. The distribution pattern of *Gad2* and *Sst* transcripts was similar between two methods on two consecutive sections (fig. S5E), as was the estimated percentage of annotated *Sst*$^+$ inhibitory neurons (fig. S5, E to G); these findings suggested that Stereo-seq data analysis at the cellular level could be similar to RNA ISH.

EGCs reside in the VZ and are responsible for neurogenesis during development and regeneration (*4*, *9*, *29*). We identified three clusters of EGCs located in distinct regions (Fig. 1F). Aside from the commonly expressed radial glia markers *Sox2*, *Gfap*, *Vim*, *Fabp7*, and *Slc1a3*, each EGC cluster was characterized by expression of specific markers such as *Wnt8b*, *Sfrp1*, or ribosome-related genes (Fig. 1, F and G, fig. S2A, and table S2). Accordingly, we named these clusters wntEGC, sfrpEGC, and ribEGC (Fig. 1, C and F). Gene Ontology analysis (table S3) revealed that cell cycle and translation-related genes were highly expressed in ribEGCs (Fig. 1H), suggesting an active proliferation property of ribEGC (*30*–*32*).

Other identified cell types included cholinergic, monoaminergic, and peptidergic neurons in the septum, neuroblasts near the lateral VZ, and choroid plexus cells and vascular leptomeningeal cells in the outer layer of the telencephalon (Fig. 1C and fig. S4). In this way, our work decodes the spatially resolved transcriptomes at single-cell resolution and cell types of axolotl telencephalon sections. The data can be browsed via the interactive data portal at https://db.cngb.org/stomics/artista.

EGC dynamics throughout axolotl telencephalon development

To investigate the cellular and molecular dynamics of axolotl brain development, we applied Stereo-seq to developmental (stage 44, 54, and 57), juvenile, adult, and metamorphosed forebrain sections (Fig. 2A). We collected cross-sections at defined positions (see Methods) to ensure that comparable samples from different developmental stages were used for Stereo-seq analysis. Spatially constrained clustering analysis revealed similar cortex structures on all analyzed sections, except for the section of stage 44, where the dorsal and medial pallia were indistinguishable (fig. S6, A and C), likely reflecting an unfinished brain region specification. Further analysis of the gene expression profiles showed a high correlation of defined regions among all developmental stages (fig. S6, B and D), thus suggesting comparability between sections. We next annotated these sections and identified 33 cell types in total using the unsupervised clustering analysis based on gene expression (Fig. 2A, fig. S7, and table S2). In addition to the cell types identified in Fig. 1, we discovered 13 immature/intermediate cell types, expressing both progenitor and differentiated cell markers (Fig. 2A and table S2).

We observed a dominant EGC subtype present in the VZ starting at stage 44. This subtype decreased in number from stage 54 and vanished from the juvenile stage (Fig. 2B). It expressed early developmental markers, such as *Fzd5* and *Sox1* (table S2) (*33*–*35*), and was thus named as development-related EGCs (dEGCs). sfrpEGCs and wntEGCs appeared at stage 54 and were gradually restricted to designated locations from the juvenile stage (Fig. 2, A and B). Along with dEGCs, immature neurons expressing specific markers, such as *Stmn2*, *Tubb3*, and *Dcx*, were seen at early developmental stages, yet became undetectable from the juvenile stage onward (Fig. 2, A and B, fig. S7, and table S2). The developmental neuroblasts (dNBLs) highly expressing marker genes *Nes* and *Cdkn1c* emerged with developmental timing similar to that of dEGCs and immature neurons (Fig. 2, A and B, fig. S7, and table S2), indicating a potential lineage transition from EGCs to neuroblasts and immature neurons as previously suggested (*29*). In contrast, mature neurons started to appear at stage 57, and their spatial distribution at the juvenile stage became similar to that in the adult telencephalon (Fig. 2, A and B, and fig. S7). These results indicate that the cell type and distribution in the axolotl telencephalon were established since the juvenile stage (*3*).

To characterize the molecular dynamics of EGCs during development, we evaluated the expression of composite gene modules defining neural stemness, cell cycle, and translation activity to reveal the proliferative and differentiative potential of EGCs (Methods and table S4) (*32*, *36*). Overall, cells in the expanded VZ at early developmental stages expressed high levels of all three gene modules, in line with active stem cell activities, and showed less neuron maturation during the fast brain expansion phase (Fig. 2C) (*37*). From the juvenile stage onward, cells positive for these modules dropped in number and became restricted to a thinner ventral area of the VZ (Fig. 2C), where ribEGCs were located (Fig. 1H).

Cell dynamics and cell-cell communication during regeneration

Although axolotls are capable of regenerating damaged brains (*9*), the cell types responsible for regeneration, their origins, and the molecular events that direct regenerative functions of these cells remain elusive. To tackle these questions, we first removed a portion of the dorsal pallium of the left telencephalic hemisphere following an established protocol (*9*). We then collected sections at 2, 5, 10, 15, 20, 30, and 60 days post-injury (DPI) for Stereo-seq analyses to dissect both immediate wound responses and later regeneration processes (Fig. 3A). We annotated 28 cell types across

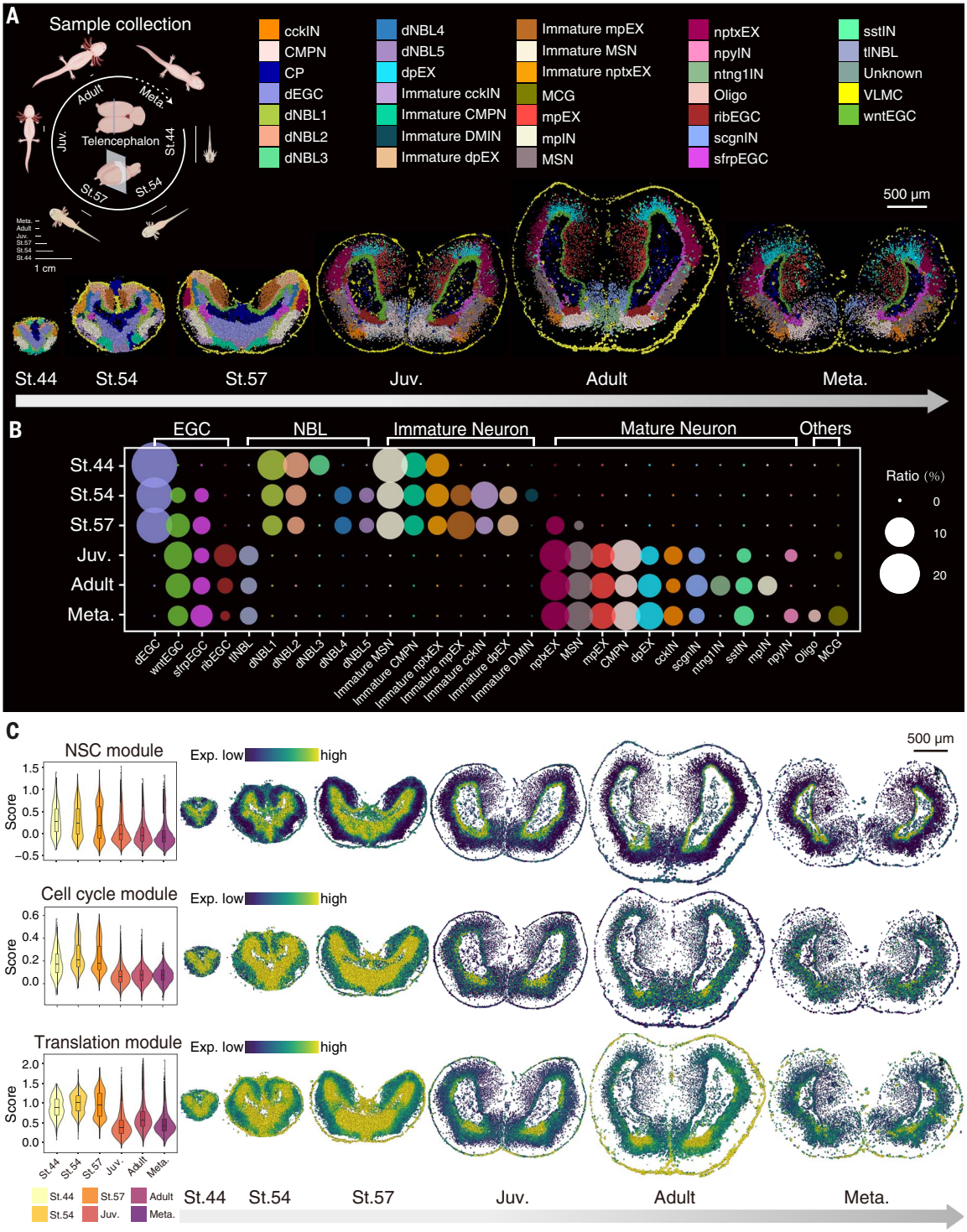

Fig. 2. Cell dynamics of axolotl telencephalon during development. (**A**) Schematic diagram of sample collection (left). Unsupervised clustering of the axolotl telencephalon sections at stage44 (St.44), stage54 (St.54), stage57 (St.57), juvenile (Juv.), Adult, and metamorphosis (Meta.). dEGC, developmental EGC; dNBL, developmental neuroblast; DMIN, dopaminergic periglomerular inhibitory neuron; MCG, microglial cell; npyIN, *Npy*$^{+}$ inhibitory neuron; ntng1IN, Oligo, oligodendrocyte. (**B**) Bubble plot showing the ratio of individual cell types in the axolotl telencephalon at different developmental stages, including St.44, St.54, St.57, Juv., Adult, and Meta. (**C**) Violin plot (left) and spatial visualization (right) of gene modules, the expression level of which defines neural stem cell (NSC), cell cycle, and translation captured by Stereo-seq at different developmental stages in the axolotl telencephalon.

sections using established marker genes, eight of which were not previously seen in development (Fig. 3B, fig. S9, A and B, and table S2). To assess the reproducibility of our data, we integrated Stereo-seq data of multiple neighboring sections along the anterior-posterior axis at 2, 5, 10, 15, and 20 DPI. The results showed that both cell type composition and the gene expression profile of each cell type for all sections of same stage were highly consistent with each other, and were therefore integrated for downstream analysis (fig. S8). The series Stereo-seq data revealed that morphological recovery from the injury occurred within 30 days, as previously reported (*9*). At 60 DPI, we observed that the cell types and their distribution were fully restored (Fig. 3B).

To identify injury-responding cells, we investigated the dynamics of 14 major cell types by calculating the ratio of each cell population in the injured versus uninjured site at seven regeneration stages (Fig. 3C and fig. S10) (see Methods). Two types of cells increased in number from 2 DPI and maintained their population until 15 DPI. One population was microglia cells expressing makers *C1qb* and *Ctsl*, which likely were recruited to participate in the inflammatory response (Fig. 3, C and D, and table S2) (*38*). The other population was a type of EGC that expressed higher

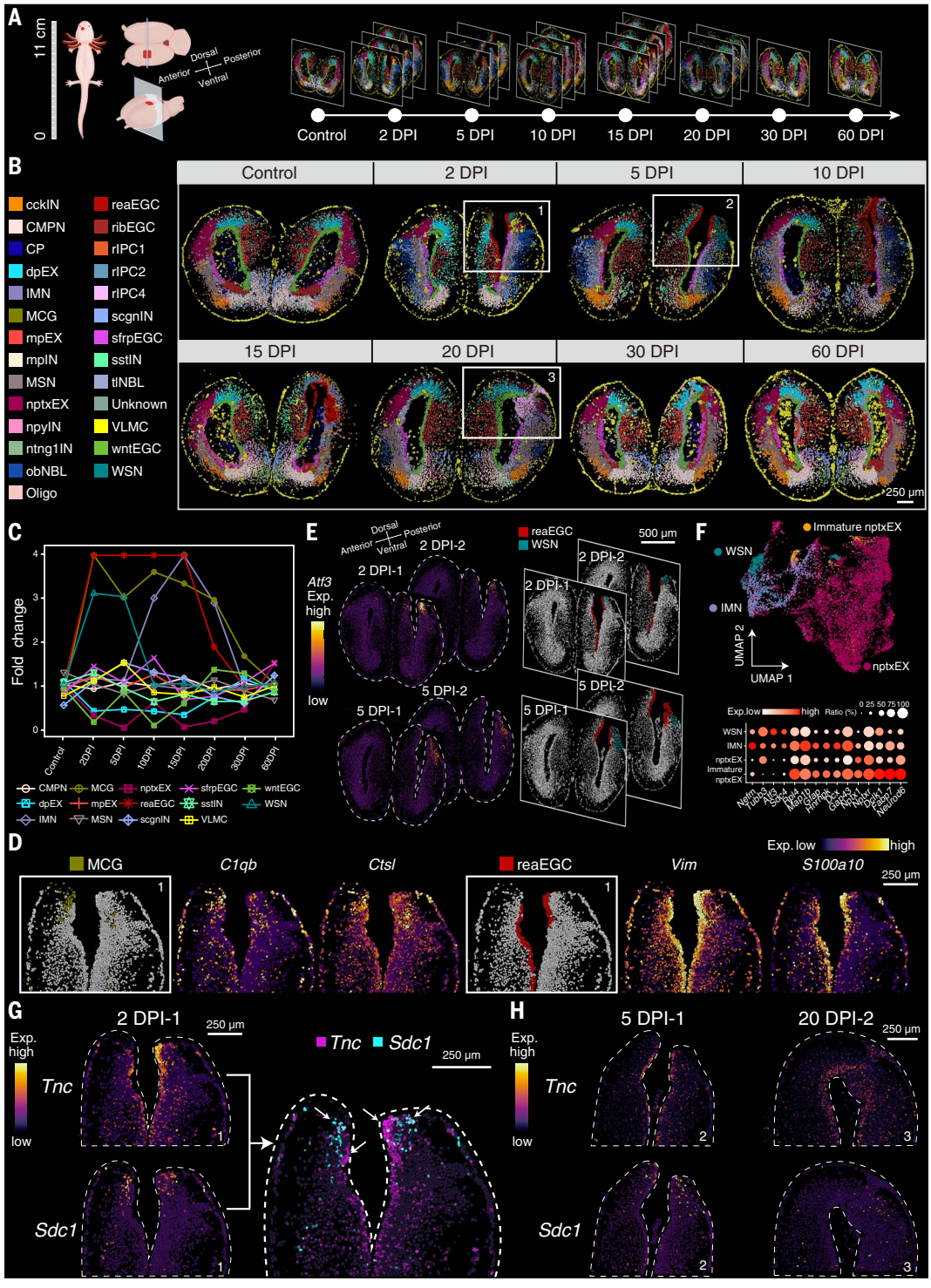

Fig. 3. Spatiotemporal transcriptomics of axolotl brain during regeneration. (**A**) Schematic diagram of sample collection (left). Overview of the sampled sections at homeostatic and regenerative stages (right). (**B**) Spatial visualization of cell types identified in the axolotl telencephalon sections by Stereo-seq at different stages of regeneration. IMN, immature neuron; obNBL, olfactory bulb neuroblast; reaEGC, reactive EGC; rIPC, regeneration intermediate progenitor cell; WSN, wound-stimulated neuron. (**C**) Line graph showing the fold change of the cell ratio in the injured hemisphere compared to the uninjured hemisphere across all stages. We set 4 as the maximum fold-change value for better visualization in the line plot. (**D**) Spatial visualization of marker gene expression in MCGs (left) and reaEGCs (right) on the 2 DPI section. (**E**) Spatial visualization of the expression level of *Atf3* and the distribution of reaEGCs and WSNs on the sections of 2 DPI and 5 DPI. (**F**) UMAP visualization of the segmented cells from the dorsal regions of developmental stages (St.44, St.54, St.57) and regenerative stages (2 to 20 DPI), including nptxEX from both processes, immature nptxEX from developmental stages, and IMN and WSN from regenerative stages. Cells are colored according to cell type annotation (top). Bubble plot showing the expression levels of the specific markers of these four cell types (bottom). (**G** and **H**) Spatial visualization of the expression level of a ligand-receptor pair (*Tnc* and *Sdc1*) on the sections of 2, 5, and 20 DPI.

levels of glial cell markers (such as *Vim*) than other EGC subtypes during homeostasis, as well as a unique marker, *S100a10* (Fig. 3D). Thus, it was named as reactive EGCs (reaEGCs) (Fig. 3, C and D, and table S2). Monocle analysis of the sections at 2 DPI indicated that reaEGCs in medial and lateral pallium regions likely originated from local wntEGCs and sfrpEGCs, respectively (fig. S11, A and B). Further investigation by Monocle2 analysis revealed a group of genes, including several transcription factors, exhibiting patterned expression changes along the pseudotime axis from wntEGCs or sfrpEGCs to reaEGCs (fig. S11, C and D). The predicted regulatory networks and pathways of these transcription factors were related to neural precursor cell proliferation and differentiation (fig. S11D). Moreover, our WGCNA analysis highlighted four transcription factors specifically coexpressed in reaEGCs (fig. S11E), which are part of regulatory pathways involved in the wound-healing response (fig. S11, F and G). In sum, these results suggest that reaEGCs induced immediately upon injury may have a positive role in regeneration.

In addition, we observed a group of neurons that were transiently induced at 2 and 5 DPI

and highly expressed the neuron growth contributor *Atf3* (Fig. 3, C and E) (*39*). Their transcriptomic profile was distinct from that of location-matched nptxEXs on the uninjured hemisphere of the telencephalon, but was similar to that of immature neurons (IMN) appearing from 10 to 20 DPI. This group of neurons was thus named as wound-stimulated neurons (WSNs) (Fig. 3F). The genes *Dclk1* and *Gap43* involved in neuron maturation and axonal growth were both up-regulated in expression, whereas genes enriched in mature neurons, such as *Nptx1* and *Neurod6*, were down-regulated in WSNs relative to nptxEXs (Fig. 3F). Considering (i) the identical location of WSNs and nptxEXs before injury, and (ii) the immediate appearance of WSNs at 2 DPI before regenerative neurogenesis (Fig. 3C) (*40*), we speculated that WSNs were derived from the local nptxEXs via a transcriptomic remodeling response to injury, reminiscent of the observation for corticospinal and somatosensory neurons after nerve injury in rodents (*41*, *42*). Our results indicate that the neuronal identity may be remodeled into a rejuvenated state upon injury in the axolotl brain.

The communication between cells in the local microenvironment is pivotal for coordinated regeneration responses (*43*). To examine cell-cell communication during the early regeneration period, we divided the 2 DPI section into 10 regions according to spatially constrained clustering analysis and predicted potential ligand-receptor interactions in each region. We found that the majority of detected interacting ligand-receptor pairs were in the VZ and were involved in proliferation, cell migration, and extracellular matrix remodeling, suggesting an active EGC response to injury (fig. S11H). We observed strong expression of *Tnc* and *Sdc1* as well as a high interaction score in adjacent clusters of reaEGCs and WSNs at the wound edge (Fig. 3, G and H, and fig. S11H). TNC is a glycoprotein in adult neurogenic niches required for tissue repair and regeneration (*44*). SDC1 is also shown to be induced by injury and participate in neurogenesis (*45*). These data collectively indicate a regulatory role of reaEGCs for injured neurons during regeneration (Fig. 3, B, G, and H).

Cell lineage dynamics during regenerative neurogenesis

The observation of reaEGCs at the wound site elicits a hypothesis that this progenitor cell cluster is responsible for restoring lost neurons, particularly nptxEXs. If so, intermediate cell clusters between reaEGCs and nptxEXs in terms of differentiation state would be expected. To test this idea, we first performed saturated BrdU labeling in the injured brain of axolotls and analyzed sections at 20 DPI to mark all newly generated cells (fig. S12A). Immature neurons were then immunolabeled using antibody to TUBB3. We found that a layer of cells adjacent to polarized EGCs were positive for both BrdU and TUBB3 (fig. S12B), indicating the presence of newly generated immature neurons in the wounding/regenerating zone next to EGCs.

We then examined the origin of these immature cells by analyzing sections along the anterior-to-posterior direction of the regenerating telencephalon from the same animal at 15 DPI, when the percentage of IMNs reached the peak yet the percentage of reaEGCs started to drop (Fig. 3C). Besides the section from the wound closure area shown in Fig. 3 (15 DPI–3), we included sections from the wound center (15 DPI–1), the wound edge (15 DPI–2), and the remote area (15 DPI–4) (fig. S9B). By integrating data from all four sections, 26 cell types were identified (fig. S9B). A few nptxEXs were seen, whereas reaEGCs appeared to cover the injury site on all sections (fig. S9B). We found a high-to-low spatial gradient of nptxEXs in number from the remote region (section 15 DPI–4) to the center of the wound area (section 15 DPI–1) (fig. S9B), consistent with previous MRI scanning data for axolotl brain regeneration (*9*). These results suggest that the reconstitution of lost neurons probably occurs along with the conjunction of the injury edge, through a process that may be initiated in the peripheral region and progresses toward the center of the incision.

We noticed on section 15 DPI–4 that nptxEXs were in regions adjacent to IMNs, suggesting a potential transition between them (fig. S9B). We also observed a regeneration-specific cell cluster situated between reaEGCs and IMNs (fig. S9B), expressing markers of both reaEGCs (*Vim*, *Nes*, *Krt18*, and *S100a10*) and IMNs (*Ankrd1*, *Stmn4*, and *Nptx1*) (Fig. 4, A and B, and table S2). We therefore named this cell cluster regeneration rIPC1 (intermediate progenitor cells 1). The expression level and signal wave of reaEGC and IMN marker genes across cell layers matched the cell type distribution on the Stereo-seq map, further supporting the four–cell state organization (fig. S13, A to D). In addition, expression of cyclin inhibitors *Cdkn1a* and *Cdkn1c* was sequentially increased from reaEGCs to rIPC1s and immature nptxEXs; this finding suggests that the proliferation potential was reduced along this potential cell state transition axis (Fig. 4A) (*46*–*48*).

To further verify this transition, we divided the 15 DPI–4 section into three regions (Fig. 4C), and applied cell type–based and vector field–based RNA Velocity and Monocle pseudotime analyses in these areas (Fig. 4, D and E) (*49*). The results of both analyses supported the putative lineage transition along the reaEGC-rIPC1-IMN-nptxEX axis. Similar transitions were observed on sections 15 DPI–2 and –3 (fig. S14, A to D and G to J). We then analyzed genes with expression changes along the vector field–based pseudotime axis (Fig. 4F and fig. S14, E and K) and observed matched expression dynamics and gene functions with the potential transition, such as descending expression of stemness marker *Nes* and ascending expression of *Cdkn1c* along the axis (Fig. 4G and fig. S14, F and L).

Next, temporal analysis was performed to verify the above spatial analysis–based findings. The presumed nptxEX regeneration-related cells, including reaEGCs, rIPCs, IMNs, and nptxEXs (Fig. 4H, left panel), from 2 DPI to 60 DPI were selected to construct a pseudotime trajectory via Monocle3 (Fig. 4H, bottom right panel). The predicted lineage transition of these cells along pseudotime also supported the reaEGC-rIPC-IMN-nptxEX pattern (Fig. 4H, top right panel). We then coordinated the pseudotime trajectory result with our Stereo-seq sections during regeneration, leading to a match between pseudotime and real-time data (Fig. 4I). In summary, our results depict a scenario in which reaEGCs proliferate to cover the wound, meanwhile converting or differentiating into intermediate and mature neurons for tissue regeneration.

Comparison of developmental and regenerative neurogenesis

We noticed that the cell layer organization in the regenerating telencephalon was similar to that in the developing brain (Fig. 2A). dEGCs, dNBLs (similar to IPCs), and immature nptxEXs arrayed from the VZ to the pallium region were first observed as early as stage 44 (Fig. 5, A and B, and fig. S7). When the mature nptxEXs appeared at stage 57, four cell types of dEGCs, dNBLs, immature nptxEXs, and nptxEXs were arranged in a spatial pattern matching that on the section 15 DPI–4, thus suggesting that nptxEX regeneration may recapitulate the nptxEX development process (Fig. 5, A and B). To test this possibility, we calculated the correlation of EGCs in the dorsal left telencephalon from developmental stages 44, 54, 57, and juvenile, as well as 15 DPI–4 sections. Indeed, relative to other EGC types, the global gene expression signature of reaEGCs was most closely correlated with dEGCs at stage 57 (Fig. 5C); for example, the spatial distribution of markers such as *Nes* and *Nptx1* was similar between 15 DPI–4 and stage 57 (Fig. 4, A and B, and Fig. 5, D and E). Consistently, both RNA velocity and Monocle analyses simulated parallel lineage transition trajectories to generate nptxEXs in both developmental and regenerative processes, from EGCs to IPCs, then to immature and mature neurons (Fig. 5, F to H, fig. S15, A to C, and fig. S16, A to C).

We further assessed the molecular dynamics of these two potential transition processes using data from stage 57 and 15 DPI–4. Differentially

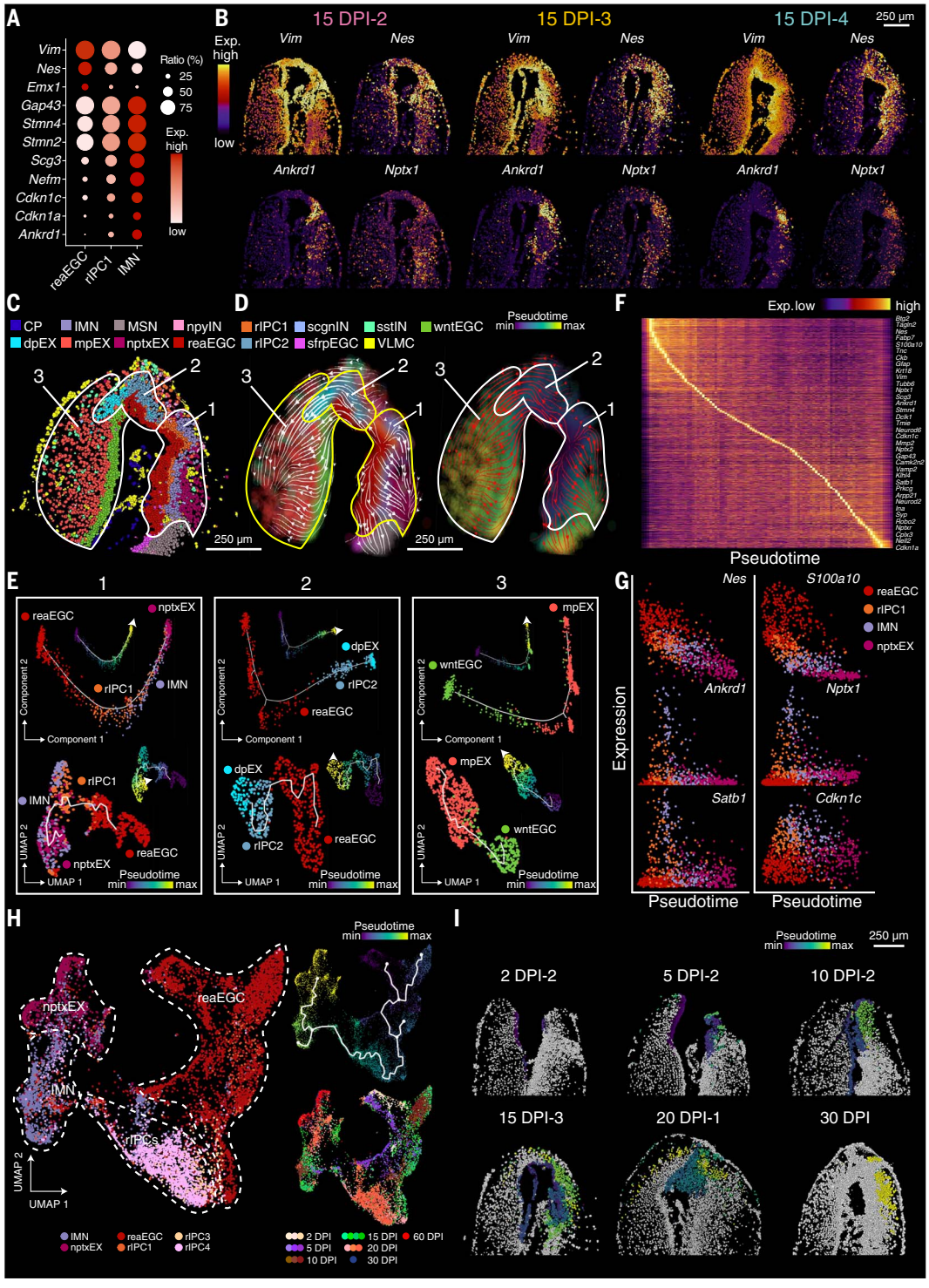

Fig. 4. Putative cell lineage transition during telencephalon regeneration. (**A**) Bubble plot reflecting the expression dynamics of marker genes defining reaEGC, rIPC1, and IMN, which are major cell types involved in axolotl telencephalon regeneration. (**B**) Spatially visualized heatmap showing the expression pattern of key markers for regeneration-related cells in the injury area of sections, including 15 DPI–2, 15 DPI–3, and 15 DPI–4 cells. (**C**) Spatial distribution of cell types around the regenerating site on the section of 15 DPI–4. (**D**) RNA velocity streamline plots showing the predicted trajectory of cell lineage transition in the regenerating region of axolotl telencephalon in 15 DPI–4 cells. Areas are colored by either annotated cell clusters (left) or pseudotime (right). (**E**) Pseudotime trajectory analysis corresponding to the three designated areas in (C), via Monocle2 (top) and Monocle3 (bottom). Cells are colored by cell type or pseudotime. (**F**) Heatmap showing pseudotemporal transition of the expression level of representative genes in regeneration. (**G**) Scatterplot showing pseudotime dynamics of the expression of *Nes*, *S100a10*, *Ankrd1*, *Nptx1*, *Satb1*, and *Cdkn1c* in clusters of reaEGC, rIPC1, IMN, and nptxEX cells. (**H**) UMAP visualization of the regeneration-related cells across regenerative stages. Cells are colored by cell type annotation (left), pseudotime (top right), and stages (bottom right). (**I**) Spatial visualization of cells in (H) with the pseudotime score in the cell lineage transition process. Cells are colored by the pseudotime score.

expressed genes were classified into eight groups with either similar or opposite trends along each process (Fig. 5I and table S5). Pathways involved in neuronal differentiation, migration, maturation, communication, and synaptic activities were up-regulated in both processes. In contrast, pathways related to proliferation, cell cycle progression, and related molecular events, such as translation initiation and RNA splicing, were down-regulated (Fig. 5J). These results agree with the consensus that stemness and proliferation activity decline during neurogenesis (Fig. 5J). Our analysis also showed that chromatin organization, TOR signaling, and transcriptional regulation by TP53 were specifically up-regulated during the transition process in regeneration, suggesting possible metabolic and genome stability control for the rapid cell growth during regeneration (*50*, *51*). In addition, we observed a regeneration-specific rise of autophagy-related genes and a decline in gene expression related to wound and stress responses (Fig. 5J), possibly reflecting a transition of molecular activities from wound response in reaEGC to neuronal regeneration. In total, hundreds of regenerative-specific

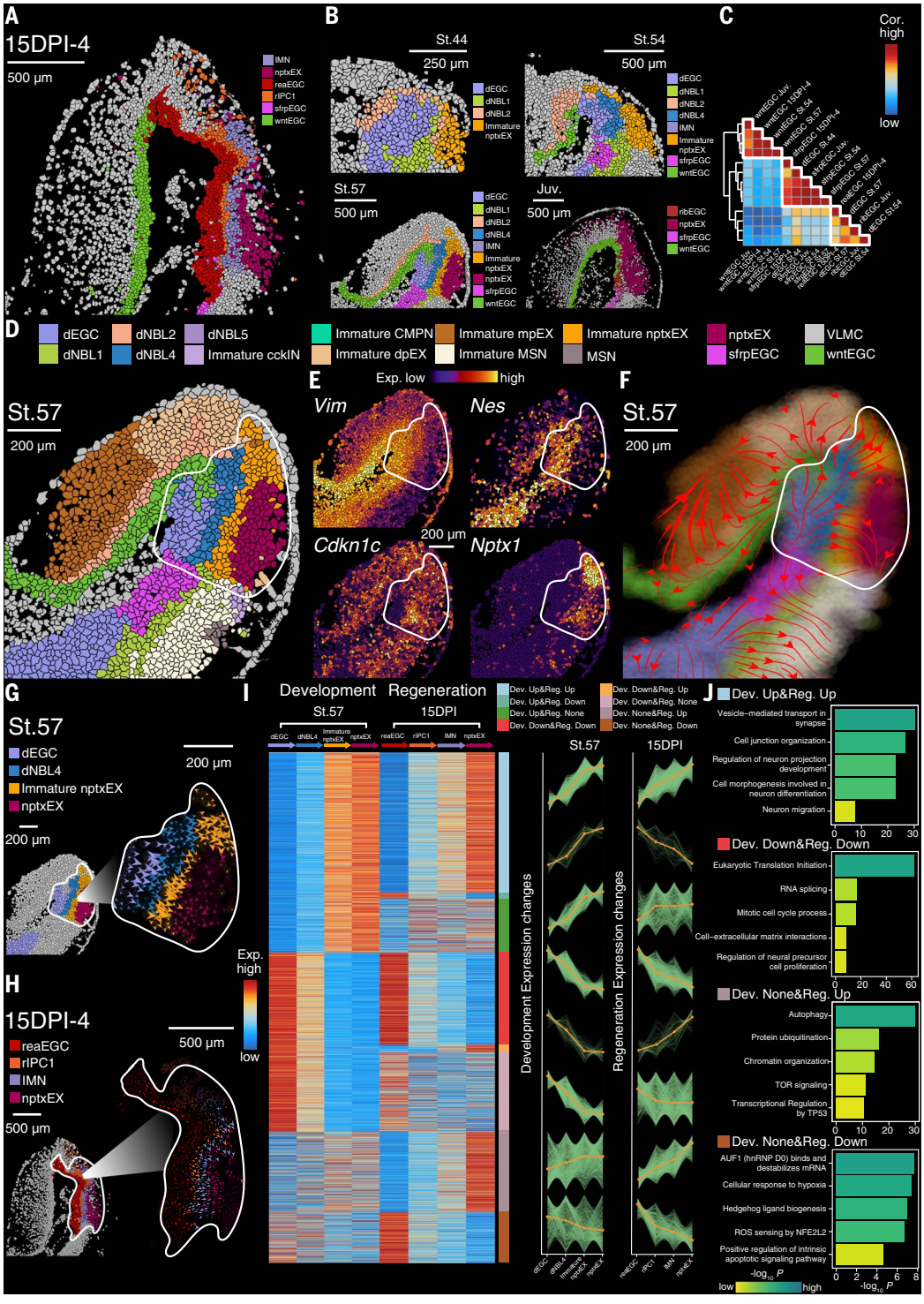

Fig. 5. Comparison of neurogenesis between development and regeneration. (**A** and **B**) Spatial distribution of major cell types in the dorsal pallium of the left hemisphere at 15 DPI–4 (A) and at St.44, St.54, St.57, and Juv. (B). (**C**) Heatmap displaying the correlation between different EGC types at 15 DPI and four developmental stages. (**D**) Spatial distribution of cell types in the dorsal pallium of the axolotl left telencephalon at St.57. Cells potentially involved in the development of nptxEX are framed by the white line. Cell types are annotated by colored cubes on top. (**E**) Spatially visualized expression of key markers on the section shown in (D). (**F**) RNA velocity streamline plot showing the predicted dorsal pallium development trajectory in the left hemisphere of the axolotl telencephalon at St.57. (**G** and **H**) RNA velocity streamline plot showing the predicted lineage transition trajectory of dEGC, dNBL, immature nptxEX, and nptxEX at St.57 (G) and reaEGC, rIPC1, IMN, and nptxEX at 15 DPI (H). (**I**) Left: Heatmap of gene expression during nptxEX development and regeneration. Eight distinct groups of genes were sorted by their dynamic expression pattern. Right: Line plot depicting standardized Stereo-seq signal by fuzzy cluster analysis for eight groups, with green lines representing the expression dynamics of individual genes and the orange line representing the integrated pattern of each group of genes at St.57 or 15 DPI. Dev. Up, up-regulated in development; Dev. Down, down-regulated in development; Reg. Up, up-regulated in regeneration; Reg. Down, down-regulated in regeneration; None, no significant change. (**J**) Bar plot exhibiting the representative Gene Ontology enrichment pathways of groups in (I).

genes were identified by this comparison (fig. S17 and table S6).

Discussion

How EGCs contribute to brain regeneration in the amphibian remains elusive (*10*, *11*, *14*). By identifying the reaEGC subtype and presenting its dynamic functions for regeneration, our work not only supports the injury-specific activation and accumulation of EGCs with elevated proliferation capacity around the lesion (*9*, *10*), but also indicates that these cells are the origin of neurogenesis for regeneration (*9*–*11*). Moreover, our results show that reaEGCs are similar to dEGCs by whole-transcriptome comparison. As dEGCs appeared from the earliest stage of development sampled in our study, and presumably gave rise to other EGC types and neurons, they may possess a more pluripotent potential than EGCs in the adult brain. Therefore, as a consequence of the absence of dEGCs in adulthood, our data indicate that reaEGCs may originate from non-dEGC subtypes by reprogramming.

In regard to the cellular origin of reaEGCs, we identified three EGC subtypes in the VZ of the adult telencephalon by whole-transcriptome

analysis and their spatial distribution. These EGC subtypes retained expression of neural stem cell and cell cycle markers, similar to EGCs and radial glial cells previously identified in newts and zebrafish, respectively (*2*, *10*). Our trajectory analysis suggested that reaEGCs were closer to sfrpEGCs and wntEGCs than to ribEGCs. Moreover, we showed that subpopulations of reaEGCs in the medial pallium, lateral pallium, and VZ not only expressed low levels of *Wnt* and *Sfrp*, but also expressed transcription factors that regulate glial cell proliferation and differentiation pathways, suggesting a direct lineage relationship between these EGC populations. In addition, reaEGCs occupied a large area in the VZ of the injured hemisphere at early regeneration stages, where wntEGCs or sfrpEGCs were originally located. Taken together, these findings indicate that reaEGCs may originate mainly from local wntEGCs and sfrpEGCs.

However, we still cannot rule out the possibility that reaEGCs originate from other regions of the axolotl brain and migrate to the wound site. Although we observed few ribEGCs at the dorsal pallium, this type of cell retains active expression of proliferation-related genes. The possibility remains that some ribEGCs proliferate and migrate to the wound area, through which they contribute to the induction of reaEGCs. VZ-specific labeling and functional perturbation assays will be required if we are to elucidate how EGCs in different regions function during regeneration.

Our work has redefined EGC subpopulations and revealed their dynamics and roles in development and regeneration. Injury-induced regeneration also requires collaborative activities of cells in different regions, including cells from the olfactory bulb (*4*, *9*). Therefore, Stereo-seq data from other regions of the brain would help to enable displays of cell activities at the three-dimensional level and to investigate how cellular and molecular cues are polarized to direct regeneration.

Methods summary

In brief, the OCT embedded snap-frozen brain samples from the *d/d* strain of *Ambystoma mexicanum* at different stages of development and regeneration after dorsal telencephalon injury were used for making cryosections, which were then subjected to spatial transcriptomics library construction using Stereo-seq. Brain damage was generated by removing a square-shaped (size 0.5 mm × 0.5 mm) piece of dorsal telencephalon tissue.

Raw sequencing data were processed using the SAW pipeline (https://github.com/BGIResearch/SAW). High-quality mapped reads were annotated and calculated to generate a CID-containing expression profile matrix by handleBam (*52*). To generate the expression matrix at single-cell resolution by Stereo-seq, the DNB image was first manually registered with nucleic acid staining images. The Scikit-image package was then used to perform single-cell segmentation after removing background and computing Euclidean distances of stained images (*53*). UMIs from all DNBs in the same putative single cell were aggregated per gene and summed to generate a gene expression matrix for downstream analysis.

Seurat was used for quality control, SCT normalization, dimensionality reduction, clustering, and identification of marker genes (*28*). Sections along the anterior-posterior axis were integrated by the canonical correlation analysis (CCA) algorithm in the Seurat package. Telencephalon region definition was achieved by combining spatially constrained clustering and morphological information. Cell type identification was performed based on known marker gene sets and verified by in situ hybridization experiments. Newly born neurons were traced by cumulative BrdU labeling and immunohistochemistry.

To capture the cell transition trajectories at the spatial level, the raw count matrix was established according to the annotated bam file and Dynamo was used to perform RNA velocity analysis with unspliced and spliced RNA transcripts (*49*, *52*). For modeling and further clarifying different trajectories on the same section, Monocle2 and Monocle3 were used to perform pseudotime analysis with selected cell types involved in specific developmental or regenerative processes (*54*, *55*). For modeling trajectories across regeneration stages, RPCA with SCT-normalized data was used to integrate regeneration-related cell types across regeneration stages, and Monocle3 analysis was then performed downstream.

See the supplementary materials for further details.

REFERENCES AND NOTES

1. E. M. Tanaka, P. Ferretti, Considering the evolution of regeneration in the central nervous system. *Nat. Rev. Neurosci.* **10**, 713–723 (2009). doi: 10.1038/nrn2707; pmid: 19763104
2. V. Kroehne, D. Freudenreich, S. Hans, J. Kaslin, M. Brand, Regeneration of the adult zebrafish brain from neurogenic radial glia-type progenitors. *Development* **138**, 4831–4841 (2011). doi: 10.1242/dev.072587; pmid: 22007133
3. A. Joven, A. Simon, Homeostatic and regenerative neurogenesis in salamanders. *Prog. Neurobiol.* **170**, 81–98 (2018). doi: 10.1016/j.pneurobio.2018.04.006; pmid: 29654836
4. M. Maden, L. A. Manwell, B. K. Ormerod, Proliferation zones in the axolotl brain and regeneration of the telencephalon. *Neural Dev.* **8**, 1 (2013). doi: 10.1186/1749-8104-8-1; pmid: 23327114
5. K. Lust, E. M. Tanaka, A Comparative Perspective on Brain Regeneration in Amphibians and Teleost Fish. *Dev. Neurobiol.* **79**, 424–436 (2019). doi: 10.1002/dneu.22665; pmid: 30600647
6. T. Gerber *et al*., Single-cell analysis uncovers convergence of cell identities during axolotl limb regeneration. *Science* **362**, eaaq0681 (2018). doi: 10.1126/science.aaq0681; pmid: 30262634
7. H. Li *et al*., Dynamic cell transition and immune response landscapes of axolotl limb regeneration revealed by single-cell analysis. *Protein Cell* **12**, 57–66 (2021). doi: 10.1007/s13238-020-00763-1; pmid: 32748350
8. H. S. Burr, Regeneration in the brain of amblystoma. I. The regeneration of the forebrain. *J. Comp. Neurol.* **26**, 203–211 (1916). doi: 10.1002/cne.900260203
9. R. Amamoto *et al*., Adult axolotls can regenerate original neuronal diversity in response to brain injury. *eLife* **5**, e13998 (2016). doi: 10.7554/eLife.13998; pmid: 27156560
10. M. Kirkham, L. S. Hameed, D. A. Berg, H. Wang, A. Simon, Progenitor cell dynamics in the Newt Telencephalon during homeostasis and neuronal regeneration. *Stem Cell Rep.* **2**, 507–519 (2014). doi: 10.1016/j.stemcr.2014.01.018; pmid: 24749074
11. D. A. Berg *et al*., Efficient regeneration by activation of neurogenesis in homeostatically quiescent regions of the adult vertebrate brain. *Development* **137**, 4127–4134 (2010). doi: 10.1242/dev.055541; pmid: 21068061
12. D. Ryczko, A. Simon, A. J. Ijspeert, Walking with Salamanders: From Molecules to Biorobotics. *Trends Neurosci.* **43**, 916–930 (2020). doi: 10.1016/j.tins.2020.08.006; pmid: 33010947
13. A. González, J. M. López, R. Morona, N. Moreno, in *Evolution of Nervous Systems*, J. H. Kaas, Ed. (Academic Press, 2017), vol. 1, chap. 8.
14. A. Joven *et al*., Cellular basis of brain maturation and acquisition of complex behaviors in salamanders. *Development* **145**, dev160051 (2018). pmid: 29217751
15. N. Kishimoto, K. Shimizu, K. Sawamoto, Neuronal regeneration in a zebrafish model of adult brain injury. *Dis. Model. Mech.* **5**, 200–209 (2012). doi: 10.1242/dmm.007336; pmid: 22028327
16. C. Kizil *et al*., Regenerative neurogenesis from neural progenitor cells requires injury-induced expression of Gata3. *Dev. Cell* **23**, 1230–1237 (2012). doi: 10.1016/j.devcel.2012.10.014; pmid: 23168169
17. V. Marx, Method of the Year: Spatially resolved transcriptomics. *Nat. Methods* **18**, 9–14 (2021). doi: 10.1038/s41592-020-01033-y; pmid: 33408395
18. C. Ortiz *et al*., Molecular atlas of the adult mouse brain. *Sci. Adv.* **6**, eabb3446 (2020). doi: 10.1126/sciadv.abb3446; pmid: 32637622
19. K. R. Maynard *et al*., Transcriptome-scale spatial gene expression in the human dorsolateral prefrontal cortex. *Nat. Neurosci.* **24**, 425–436 (2021). doi: 10.1038/s41593-020-00787-0; pmid: 33558695
20. C. L. Eng *et al*., Transcriptome-scale super-resolved imaging in tissues by RNA seqFISH. *Nature* **568**, 235–239 (2019). doi: 10.1038/s41586-019-1049-y; pmid: 30911168
21. C. Xia, J. Fan, G. Emanuel, J. Hao, X. Zhuang, Spatial transcriptome profiling by MERFISH reveals subcellular RNA compartmentalization and cell cycle-dependent gene expression. *Proc. Natl. Acad. Sci. U.S.A.* **116**, 19490–19499 (2019). doi: 10.1073/pnas.1912459116; pmid: 31501331
22. A. Chen *et al*., Spatiotemporal transcriptomic atlas of mouse organogenesis using DNA nanoball-patterned arrays. *Cell* **185**, 1777–1792.e21 (2022). doi: 10.1016/j.cell.2022.04.003; pmid: 35512705
23. G. Roth, W. Walkowiak, The Influence of Genome and Cell Size on Brain Morphology in Amphibians. *Cold Spring Harb. Perspect. Biol.* **7**, a019075 (2015). doi: 10.1101/cshperspect.a019075; pmid: 26261281
24. C. J. Herrick, *The Brain of the Tiger Salamander*, Ambystoma tigrinum (Univ. of Chicago Press, 1948).
25. R. Drmanac *et al*., Human genome sequencing using unchained base reads on self-assembling DNA nanoarrays. *Science* **327**, 78–81 (2010). doi: 10.1126/science.1181498; pmid: 19892942
26. D. Gaidatzis, L. Burger, M. Florescu, M. B. Stadler, Analysis of intronic and exonic reads in RNA-seq data characterizes transcriptional and post-transcriptional regulation. *Nat. Biotechnol.* **33**, 722–729 (2015). doi: 10.1038/nbt.3269; pmid: 26098447
27. I. Lazcano *et al*., MRI- and histologically derived neuroanatomical atlas of the Ambystoma mexicanum (axolotl). *Sci. Rep.* **11**, 9850 (2021). doi: 10.1038/s41598-021-89357-3; pmid: 33972650
28. Y. Hao *et al*., Integrated analysis of multimodal single-cell data. *Cell* **184**, 3573–3587.e29 (2021). doi: 10.1016/j.cell.2021.04.048; pmid: 34062119
29. S. C. Noctor, A. C. Flint, T. A. Weissman, R. S. Dammerman, A. R. Kriegstein, Neurons derived from radial glial cells establish radial units in neocortex. *Nature* **409**, 714–720 (2001). doi: 10.1038/35055553; pmid: 11217860
30. W. Niu *et al*., SOX2 reprograms resident astrocytes into neural progenitors in the adult brain. *Stem Cell Rep.* **4**, 780–794 (2015). doi: 10.1016/j.stemcr.2015.03.006; pmid: 25921813
31. M. Barna, Ribosomes take control. *Proc. Natl. Acad. Sci. U.S.A.* **110**, 9–10 (2013). doi: 10.1073/pnas.1218764110; pmid: 23243144

32. S. Temple, The development of neural stem cells. *Nature* **414**, 112–117 (2001). doi: 10.1038/35102174; pmid: 11689956
33. C. J. Burns *et al*., Investigation of Frizzled-5 during embryonic neural development in mouse. *Dev. Dyn.* **237**, 1614–1626 (2008). doi: 10.1002/dvdy.21565; pmid: 18489003
34. D. M. Suter, D. Tirefort, S. Julien, K. H. Krause, A Sox1 to Pax6 switch drives neuroectoderm to radial glia progression during differentiation of mouse embryonic stem cells. *Stem Cells* **27**, 49–58 (2009). doi: 10.1634/stemcells.2008-0319; pmid: 18832594
35. L. H. Pevny, S. Sockanathan, M. Placzek, R. Lovell-Badge, A role for SOX1 in neural determination. *Development* **125**, 1967–1978 (1998). doi: 10.1242/dev.125.10.1967; pmid: 9550729
36. J. Fu, A. Warmflash, M. P. Lutolf, Stem-cell-based embryo models for fundamental research and translation. *Nat. Mater.* **20**, 132–144 (2021). doi: 10.1038/s41563-020-00829-9; pmid: 33199861
37. G. M. Schreckenberg, A. G. Jacobson, Normal stages of development of the axolotl. Ambystoma mexicanum. *Dev. Biol.* **42**, 391–400 (1975). doi: 10.1016/0012-1606(75)90343-7; pmid: 1167837
38. Z. Li *et al*., M-CSF, IL-6, and TGF-β promote generation of a new subset of tissue repair macrophage for traumatic brain injury recovery. *Sci. Adv.* **7**, eabb6260 (2021). doi: 10.1126/sciadv.abb6260; pmid: 33712456
39. R. Seijffers, C. D. Mills, C. J. Woolf, ATF3 increases the intrinsic growth state of DRG neurons to enhance peripheral nerve regeneration. *J. Neurosci.* **27**, 7911–7920 (2007). doi: 10.1523/JNEUROSCI.5313-06.2007; pmid: 17652582
40. A. Rodrigo Albors *et al*., Planar cell polarity-mediated induction of neural stem cell expansion during axolotl spinal cord regeneration. *eLife* **4**, e10230 (2015). doi: 10.7554/eLife.10230; pmid: 26568310
41. W. Renthal *et al*., Transcriptional Reprogramming of Distinct Peripheral Sensory Neuron Subtypes after Axonal Injury. *Neuron* **108**, 128–144.e9 (2020). doi: 10.1016/j.neuron.2020.07.026; pmid: 32810432
42. G. H. D. Poplawski *et al*., Injured adult neurons regress to an embryonic transcriptional growth state. *Nature* **581**, 77–82 (2020). doi: 10.1038/s41586-020-2200-5; pmid: 32376949
43. W. D. Snider, F.-Q. Zhou, J. Zhong, A. Markus, Signaling the pathway to regeneration. *Neuron* **35**, 13–16 (2002). doi: 10.1016/S0896-6273(02)00762-6; pmid: 12123603
44. A. Faissner, L. Roll, U. Theocharidis, Tenascin-C in the matrisome of neural stem and progenitor cells. *Mol. Cell. Neurosci.* **81**, 22–31 (2017). doi: 10.1016/j.mcn.2016.11.003; pmid: 27836730
45. M. A. Mouthon *et al*., Syndecan-1 stimulates adult neurogenesis in the mouse ventricular-subventricular zone after injury. *iScience* **23**, 101784 (2020). doi: 10.1016/j.isci.2020.101784; pmid: 33294792
46. I. Dutto, M. Tillhon, O. Cazzalini, L. A. Stivala, E. Prosperi, Biology of the cell cycle inhibitor p21(CDKN1A): Molecular mechanisms and relevance in chemical toxicology. *Arch. Toxicol.* **89**, 155–178 (2015). doi: 10.1007/s00204-014-1430-4; pmid: 25514883
47. D. Mademtzoglou *et al*., Cellular localization of the cell cycle inhibitor Cdkn1c controls growth arrest of adult skeletal muscle stem cells. *eLife* **7**, e33337 (2018). doi: 10.7554/eLife.33337; pmid: 30284969
48. F. Calegari, W. Haubensak, C. Haffner, W. B. Huttner, Selective lengthening of the cell cycle in the neurogenic subpopulation of neural progenitor cells during mouse brain development. *J. Neurosci.* **25**, 6533–6538 (2005). doi: 10.1523/JNEUROSCI.0778-05.2005; pmid: 16014714
49. X. Qiu *et al*., Mapping transcriptomic vector fields of single cells. *Cell* **185**, 690–711.e45 (2022). doi: 10.1016/j.cell.2021.12.045; pmid: 35108499
50. K. K. Park, K. Liu, Y. Hu, J. L. Kanter, Z. He, PTEN/mTOR and axon regeneration. *Exp. Neurol.* **223**, 45–50 (2010). doi: 10.1016/j.expneurol.2009.12.032; pmid: 20079353
51. M. Charni, R. Aloni-Grinstein, A. Molchadsky, V. Rotter, p53 on the crossroad between regeneration and cancer. *Cell Death Differ.* **24**, 8–14 (2017). doi: 10.1038/cdd.2016.117; pmid: 27768121
52. G. La Manno *et al*., RNA velocity of single cells. *Nature* **560**, 494–498 (2018). doi: 10.1038/s41586-018-0414-6; pmid: 30089906
53. F. Pedregosa *et al*., Scikit-learn: Machine learning in Python. *J. Mach. Learn. Res.* **12**, 2825–2830 (2011).
54. X. Qiu *et al*., Single-cell mRNA quantification and differential analysis with Census. *Nat. Methods* **14**, 309–315 (2017). doi: 10.1038/nmeth.4150; pmid: 28114287
55. J. Cao *et al*., The single-cell transcriptional landscape of mammalian organogenesis. *Nature* **566**, 496–502 (2019). doi: 10.1038/s41586-019-0969-x; pmid: 30787437
56. Y. Liu, S. Wang, W. Feng, Y. Yang, X. Wei, Codes for the paper "Single-cell Stereo-seq reveals induced progenitor cells involved in axolotl brain regeneration". https://doi.org/10.5281/zenodo.6792037 (2022). doi: 10.5281/zenodo.6792037

ACKNOWLEDGMENTS

We thank L. Bolund, G. Volpe, and I. Seim for critical reading of the manuscript. **Funding:** This work was supported by the National Key R&D Program of China (2019YFE0106700, 2021YFA0805000, 2021YFA1100500), Strategic Priority Research Program of the Chinese Academy of Sciences (Grant No. XDA16010000), the Guangdong Provincial Key Laboratory of Genome Read and Write (2017B030301011), the Shenzhen Key Laboratory of Single-Cell Omics (No. ZDSYS20190902093613831), the National Natural Science Foundation of China (32171289, 31970619, 31970782), the Innovative Research Group Program of Hubei Province (2020CFA017), the High-level Hospital Construction Project of Guangdong Provincial People's Hospital (DFJHBF202103, KJ012021012), Project of Department of Education of Guangdong Province (2018KZDXM027), Key-Area Research and Development Program of Guangdong Province (2018B030332001, 2019B030335001), and Guangdong-Hong Kong-Macao-Joint Laboratory Program (2019B121205005). **Author contributions:** X.W., Y.G., J.-F.F., X.X., L.C., and H.L. conceived the idea; Y.G., J.-F.F., X.X., L.C., and H.L. supervised the work; X.W., S.F., H.L., and J.-F.F. designed the experiments; S.F., X.L., and N.Z. performed the majority of the experiments with help from M.C., J.J., J.X., Y.Z., P.L., X.S., and C.P.; X.W., Y.L., S.W., W.F., and Y.Y. performed data analysis; M.K. and T.Y. performed database construction; Y.L., X.Q., L.W., L.H., L.C., Y.Y., X.P., S.G., A.C., M.A.E., H.Y., J.W., G.F., and L.L. gave relevant advice; H.L., Y.G., L.C., J.-F.F., and X.W. wrote the manuscript with input from all authors. **Competing interests:** The authors declare no conflicts of interest. **Data and materials availability:** All data generated in this study are freely accessible in CNGB Nucleotide Sequence Archive under accession code CNP0002068. All other data are in the main paper or the supplementary materials. All code used to analyze the data is available online at https://github.com/BGI-DEV-REG/ARTISTA (*56*). Processed data can be interactively explored and downloaded from https://db.cngb.org/stomics/artista/.

SUPPLEMENTARY MATERIALS

Submitted 8 March 2022; accepted 6 July 2022
10.1126/science.abp9444

Single-cell Stereo-seq reveals induced progenitor cells involved in axolotl brain regeneration

Xiaoyu Wei, Sulei Fu, Hanbo Li, Yang Liu, Shuai Wang, Weimin Feng, Yunzhi Yang, Xiawei Liu, Yan-Yun Zeng, Mengnan Cheng, Yiwei Lai, Xiaojie Qiu, Liang Wu, Nannan Zhang, Yujia Jiang, Jiangshan Xu, Xiaoshan Su, Cheng Peng, Lei Han, Wilson Pak-Kin Lou, Chuanyu Liu, Yue Yuan, Kailong Ma, Tao Yang, Xiangyu Pan, Shang Gao, Ao Chen, Miguel A. Esteban, Huanming Yang, Jian Wang, Guangyi Fan, Longqi Liu, Liang Chen, Xun Xu, Ji-Feng Fei, and Ying Gu

Science **377** (6610), eabp9444. DOI: 10.1126/science.abp9444

Trade-offs in brain development

Salamander brains share some, but not all, structures with the mammalian brain. They also have greater capacity to regenerate in response to damage. Three groups now come together with single-cell transcriptomics analyses that set the salamander brain in evolutionary context (see the Perspective by Faltine-Gonzalez and Kebschull). By comparing salamander brains with those of lizard, turtle, and mouse, Woych *et al*. track the evolutionary innovations that gave rise to the mammalian six-layered neocortex, which salamanders do not have. Lust *et al*. take a close look at why the axolotl brain is so much more capable of regeneration than is the mammalian brain. Finally, Wei *et al*. compare the developmental and regenerative processes in the axolotl brain. —PJH